Modeling the spatiotemporal control of cell cycle acceleration during axolotl spinal cord regeneration

Emanuel Cura Costa[1], Aida Rodrigo Albors[2], Elly M. Tanaka[3] & Osvaldo Chara[1,4]*

[1] Systems Biology Group, Institute of Physics of Liquids and Biological Systems, National Scientific and Technical Research Council, University of La Plata, La Plata, Argentina.

[2] Neural Development Group, Division of Cell and Developmental Biology, School of Life Sciences, University of Dundee, Dow Street, Dundee DD1 5EH, UK.

[3] The Research Institute of Molecular Pathology (IMP), Vienna Biocenter (VBC), Vienna, Austria

[4] Center for Information Services and High Performance Computing, Technische Universität Dresden, Dresden, Germany

* Corresponding author:

Osvaldo Chara

Center for Information Services and High Performance Computing (ZIH), Technische Universität Dresden, Nöthnitzer Straße 46, 01187 Dresden, Germany. Tel. +49 351 463-38780, E-mail: osvaldo.chara@tu-dresden.de

Systems Biology Group (SysBio), Institute of Physics of Liquids and Biological Systems (IFLySIB), National Scientific and Technical Research Council (CONICET) and University of La Plata, Calle 59 N 789, 1900 La Plata, Argentina. Tel. +54 221 4233283 Ext: 26, E-mail: ochara@iflysib.unlp.edu.ar

Web: http://sysbioiflysib.wordpress.com/

Abstract:

Axolotls are uniquely able to resolve spinal cord injuries, but little is known about the mechanisms underlying spinal cord regeneration. We found that tail amputation leads to reactivation of a developmental-like program in spinal cord ependymal cells (Rodrigo Albors *et al*., 2015). We also identified a high-proliferation zone and demonstrated that cell cycle acceleration is the major driver of regenerative growth (Rost *et al*., 2016). What underlies this spatiotemporal pattern of cell proliferation, however, remained unknown. Here, using a modelling approach supported by experimental data, we show that the proliferative response in the regenerating spinal cord is consistent with a signal that starts recruiting cells 24 hours after amputation and spreads about one millimeter from the injury. Finally, our model predicts that the observed shorter S phase can explain spinal cord outgrowth in the first four days of regeneration but after, G1 shortening is also necessary to explain outgrowth dynamics.

Introduction

The axolotl (*Ambystoma mexicanum*) has the remarkable ability to regenerate the injured spinal cord (reviewed in Freitas, Yandulskaya & Monaghan, 2019; Tazaki *et al*, 2017; Chernoff *et al*., 2003), and thus represents a unique system to study the mechanisms of successful spinal cord regeneration. Key players in this process are the ependymal cells lining the central canal of the spinal cord, which retain neural stem cell potential throughout life (Becker, Becker & Hugnot, 2018).

In earlier studies, we found that spinal cord injury in the axolotl triggers the reactivation of a developmental-like program in ependymal cells, including a switch from slow, neurogenic to fast, proliferative cell divisions (Rodrigo Albors *et al*., 2015). We showed that in the uninjured spinal cord and in the non-regenerating region of the injured spinal cord, ependymal cells divide slowly, completing a cell cycle in 14.2 ± 1.3 days. In contrast, regenerating ependymal cells speed up their cell cycle and divide every 4.9 ± 0.4 days (Rodrigo Albors *et al*., 2015) (Rost et al., 2016). By using a mathematical modeling approach, we demonstrated that the acceleration of the cell cycle is the major driver of regenerative spinal cord outgrowth and that other processes such as cell influx, cell rearrangements, and neural stem cell activation play smaller roles (Rost *et al*., 2016). We quantitatively analyzed cell proliferation in space and time and identified a high-proliferation zone that emerges 4 days after amputation within the 800 μm adjacent to the injury site and shifts posteriorly over time as the regenerating spinal cord grows (Rost *et al*., 2016)(Figure 1–figure supplement 1A). What underlies this precise spatiotemporal pattern of cell proliferation in the regenerating axolotl spinal cord, however, remains unknown. Pattern formation phenomena occurring during development can be quantitatively reproduced by invoking morphogenetic signals spreading from localized sources (Morelli *et al*., 2012). It is thus conceivable that tail amputation triggers a signal that propagates or diffuses along the injured spinal cord to speed up the cell cycle of resident cells.

In this new study, we take a modelling approach tightly supported by previous experimental data to unveil the theoretical spatiotemporal distribution such signal should have to explain the observed rate of spinal cord outgrowth in the axolotl. Our model also predicts that shortening of S phase is sufficient to explain the explosive regenerative outgrowth in the first four days of regeneration, but both S and G1 shortening are necessary to explain the outgrowth dynamics from day 4 to day 8, when most cell divisions are still self-renewing/proliferative divisions (Rodrigo Albors *et al*., 2015). Together, our results provide new clues for when and where to search for the signal/s that may be responsible for driving successful spinal cord regeneration.

Results

Model of developing spinal cord

Taking into account the symmetry of the ependymal tube and that ependymal cells organize as a pseudo-stratified epithelium (Joven & Simon, 2018), we modeled the anterior-posterior (AP) axis of the spinal cord as a row of ependymal cells (see Computational methods section for more details). We assumed that all cells are rigid spheres that proliferate with a certain cell cycle length. We modeled the proliferation dynamics as follows: we assumed that in the initial condition, each cell is in a random coordinate along its cell cycle, where the initial coordinate and the cell cycle length follow a uniform and a normal distribution, respectively. In the developing axolotl spinal cord, upon cell division, i) the daughter cells inherit the cell cycle length from the mother's normal distribution and ii) the daughter cells translocate posteriorly, displacing the cells posterior to them. This last feature of the model is the implementation of what we earlier defined as "cell pushing mechanism" (Rost *et al*., 2016). This model predicts that after a time of approximately one cell cycle length, mitotic events will occur along the AP axis, contributing to the growth of the developing spinal cord (Figure 1A).

Model of regenerating spinal cord

We modeled the amputation by removing the most posterior cells of the tissue and studied the regenerative response in the remaining N_0 cells (see Figure 1B,C, Figure 1–figure supplement 1B and Computational methods section for more details). We assumed that amputation triggers the release of a signal, which spreads over the AP axis a distance of λ μm anterior to the amputation plane and, after a time τ, recruits ependymal cells within the λ μm zone, inducing a change in their proliferation program. We notated the AP position of the most anterior cell recruited by the signal as $\xi(t)$, the recruitment limit, such that $\xi(t = \tau) = -\lambda$. In the model, all cells anterior to the cell located at $\xi(t)$ are not recruited and continue cycling slowly during the simulations (Figure 1–figure supplement 1B). In contrast, cells posterior to $\xi(t)$, and thus located within λ μm anterior to the amputation plane, are recruited at time τ and modify their cycling according to the cell cycle phase in which they are in. Because we previously demonstrated that the length of G2 and M phase in ependymal cells do not change upon amputation (Rodrigo Albors *et al*., 2015), we assumed that recruited cells whose cell cycle coordinates belong to G2 or M when $t = \tau$ will continue cycling as before (Figure 1–figure supplement 1B). In contrast, based on our previous study showing that regenerating ependymal cells go through shorter G1 and S phases of the cell cycle than non-regenerative ependymal cells (Rodrigo Albors *et al*., 2015), we reasoned that the signal instructs recruited ependymal cells precisely to shorten G1 and S phases, effectively shortening their cell cycle. We conceived a mechanism of G1 shortening in which a certain part of this cell cycle phase is skipped. We implemented this mechanism as follows (Figure 1B,C and Figure 1–figure supplement 1B): If the recruited cell is at the beginning of G1 phase, such that its cell cycle coordinate is before certain critical coordinate $G1_{cr}$ when $t = \tau$, its cell cycle coordinate acquires the $G1_{cr}$ in the next simulation step. If the cell cycle coordinate of the recruited cell is located after $G1_{cr}$ when $t = \tau$, it continues cycling as before. This mechanism induces a partial synchronization of cells transiting through G1. Because all DNA must be duplicated for cell division to occur, we considered a different mechanism to model S phase shortening: If the cell cycle coordinate belongs to S when $t = \tau$, the new cell cycle coordinate of this cell will be proportionally mapped to the corresponding coordinate of a reduced S phase in the next simulation step (Figure 1B,C and Figure 1–figure supplement 1B). For instance, if the recruited cell is 40% into its (long) S phase when the signal

arrives, it will be in the 40% of its shorter S phase in the next simulation step. Daughter cells of recruited cells inherit short G1 and S phases from their mothers and consequently have shorter cell cycle lengths (Figure 1C). To parametrize the cell phase durations of recruited and non-recruited cells and cell geometry, we used our previous experimental data in regenerating and non-regenerating axolotl spinal cords (Rodrigo Albors *et al*., 2015)(see Computational methods section and Table 1).

The model predicts that if we wait a time similar to the reduced cell cycle length, we will observe more mitotic events posterior to ξ than anterior to it. In particular, if this model is correct, the prediction for ξ (Figure 1B) will agree with the experimental curve of the switchpoint (Figure 1-figure supplement 1A).

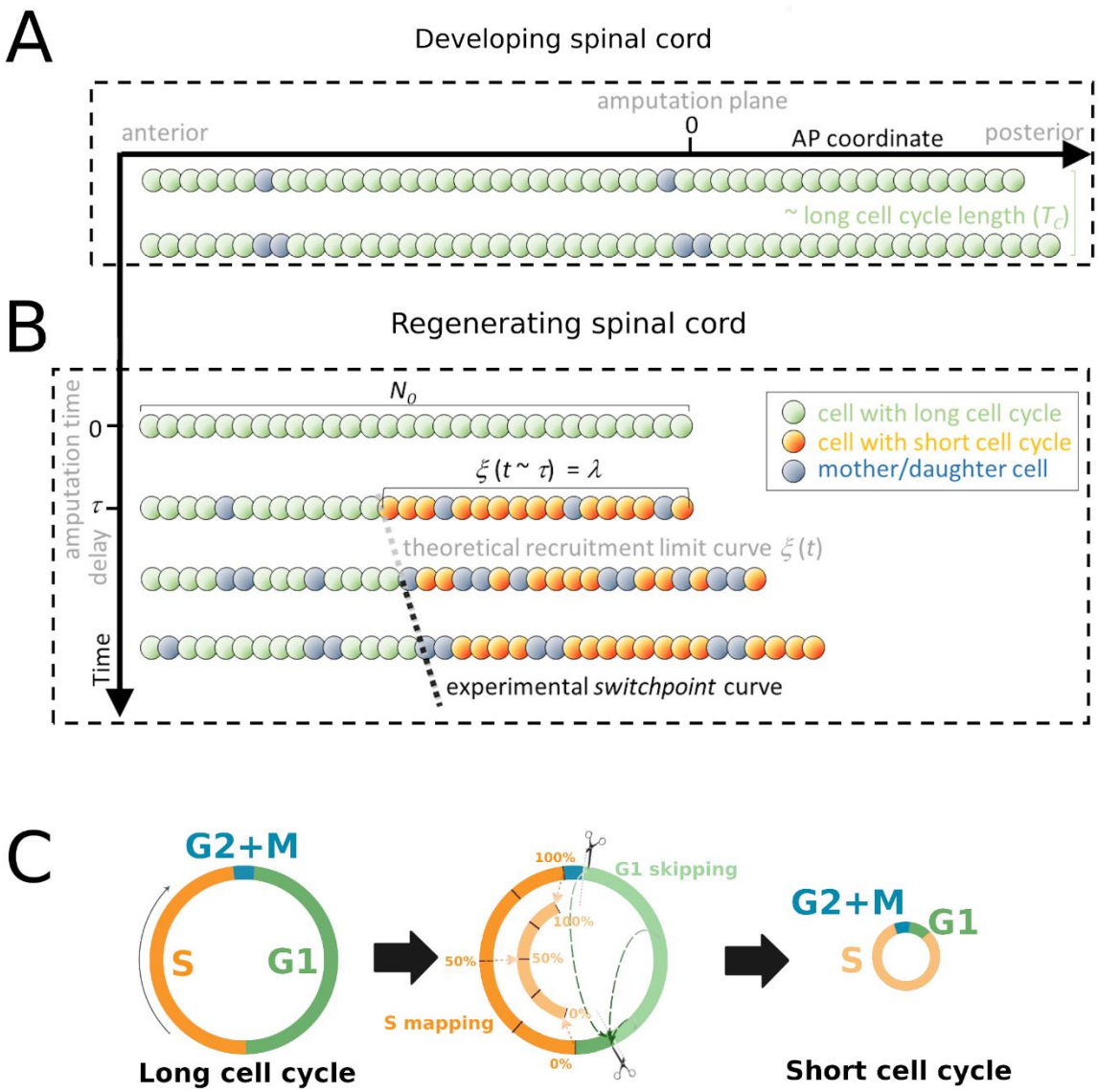

Figure 1. Model of developing and regenerating spinal cord outgrowth based on G1 and S cell phases reduction. A) Developing spinal cord. 1D model of ependymal cells aligned along the AP axis. After a time of the order of the long cell cycle length corresponding to the low-proliferation zone (see Supplementary Figure 1), mitoses "push" cells posteriorly making the spinal cord tissue. **B) Regenerating spinal cord.** Once amputation is executed (AP coordinate and time equal to zero) a signal is released anteriorly from the amputation plane after a time τ and spreads while recruiting resident ependymal cells up to the theoretical recruitment limit ξ located at λ µm from the amputation plane. After a certain time, the recruitment limit ξ overlaps the experimental switchpoint curve (See Supplementary Figure 1). **C) The mechanism of cell recruitment consists in partial synchronization through the G1 phase and proportional mapping between long and short S phases leading to shortening of G1 and S phases.** The diameter of the circles is approximately proportional to the length of the cell's cell cycle.

A signal recruiting cells within 1,050 μm from the amputation plane 24 hours after amputation can explain the regenerative ependymal tube outgrowth

To evaluate if the model could explain the regenerative outgrowth of the ependymal tube and to estimate the free parameters, we fitted $\xi(t)$ to the experimental switchpoint (Rost *et al.*, 2016). The model successfully reproduced the experimental switchpoint with best fitting parameters N_0 = 200 ependymal cells, λ = 1,050 μm and τ = 24 hours (Figure 2A, see Computational methods section). With this parameterization, we quantitatively predicted the time evolution of the regenerative ependymal tube outgrowth that was observed *in vivo* (Rost *et al.*, 2016) (Figure 2B, Movie M1). When setting to zero the delay τ between the amputation event and the recruitment effect of the signal (that is, the signal starts recruiting cells immediately upon amputation), the model-predicted outgrowth overestimates the experimental outgrowth (Figure 2–figure supplement 2A). On the contrary, increasing the delay to 8 days results in a shorter outgrowth than that observed *in vivo*/experimentally (Figure 2–figure supplement 2A). Reducing the initial recruitment distance λ to zero mimics a hypothetical case in which the signal is incapable of recruiting the cells anterior to the amputation plane (Figure2-figure supplement 2B). In terms of spinal cord outgrowth, this scenario is similar to the one in which the delay is about 8 days. Increasing λ to 1,575 μm and thus recruiting more ependymal cells, results in faster spinal cord outgrowth than *in vivo* (Figure 2–figure supplement 2B). Not surprisingly, the delay and the recruiting distance have opposite effects on the spinal cord outgrowth. These results point to a spatially and temporarily precise cell recruitment mechanism to give rise to tissue growth response during axolotl spinal cord regeneration.

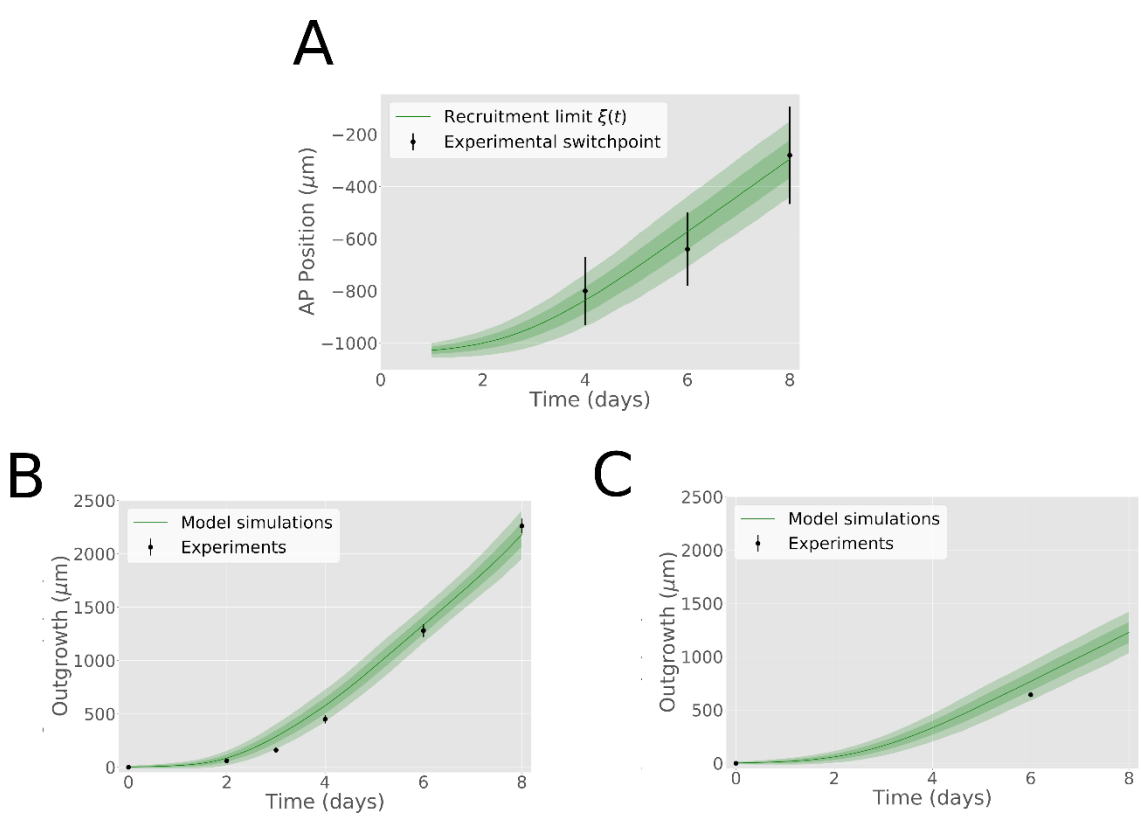

Figure 2. A signal recruiting ependymal cells from the 1,050 μm anterior to the amputation plane at 24 hours after amputation recapitulates spinal cord regenerative phenotype. A) The model of recruitment limit successfully fits the experimental switchpoint curve. Best fitting simulations of the model-predicted recruitment limit $\xi(t)$ overlap the experimental switchpoint curve. Best fitting parameters are N_0 = 200 ependymal cells, λ = 1,050 μm and τ = 24 hours. **B) The model quantitatively predicts experimental axolotl spinal cord outgrowth kinetics** (Rost *et al*., 2016). **C) The model reproduces experimental outgrowth reduction when the acceleration of cell proliferation is impeded.** Prediction of the model assuming that neither S nor G1 phase lengths were shortened superimposed with previously reported experimental outgrowth kinetics in which acceleration of the cell cycle was prevented by knocking out Sox2 (Fei *et al*., 2014). In A, B and C, lines show the means while green dark and light shaded areas correspond to 95 and 99.7 % confidence intervals, respectively, calculated from the 1,000 best fitting simulations.

Regenerating spinal cord outgrowth when acceleration of cell proliferation is impeded

According to our model, tail amputation triggers the release of a signal, which after τ hours recruits the ependymal cells within λ μm anterior to the amputation plane, shortening their G1 and S phases of the cell cycle. We asked how much the spinal cord would grow if the cell recruitment instructed by the signal is blocked. To answer this question, we made use of our model and predicted the tissue outgrowth when the length of G1 and S were unaltered. In this condition, all ependymal cells would divide with the durations of cell cycle phases reported under non-regenerating or developmental conditions (Rodrigo Albors *et al*., 2015). Our results show that blocking recruitment, and therefore the acceleration of the cell cycle, slows down tissue growth, leading to an outgrowth of 767 ± 89 μm at day 6 (Figure 2C). This result is consistent with increasing the delay τ between amputation and cell recruitment (Figure 2-figure supplement 2A) or with reducing down to zero the initial recruitment length λ (Figure 2-figure supplement 2A). Interestingly, this model-predicted outgrowth is in agreement with the reported experimental outgrowth in *Sox2* knock-out axolotls, in which the acceleration of the cell cycle does not happen in regenerating conditions (Figure 2C, Fei *et al*., 2014).

The cell pushing mechanism: the more posterior a cell is, the faster it moves

To investigate in detail the spatial distribution of cell identities along the AP axis during the regenerative response, we performed a clonal analysis in our model. To do so, we tracked the AP coordinates of cell clones throughout the model simulations by monitoring the mean AP position of cells originated from the same clone. We observed that while the anterior-most cells are slightly displaced, cells located close to the amputation plane end up at the posterior end of the regenerated spinal cord (Figure 3A), in agreement with experimental cell trajectories during axolotl spinal cord regeneration (Rost *et al*., 2016). Additionally, the velocity of a clone monotonically increases with its AP coordinate (Figure 3B), in line with experimental data (Rost *et al*., 2016). These results suggest that cells preserve their relative position along the AP axis. Hence, when plotting the relative position of each clone to the outgrowth of the corresponding tissue minus the recruitment limit $\xi(t)$, we observed that this normalized quantity is conserved in time, a fingerprint of scaling behavior (Figure 3C).

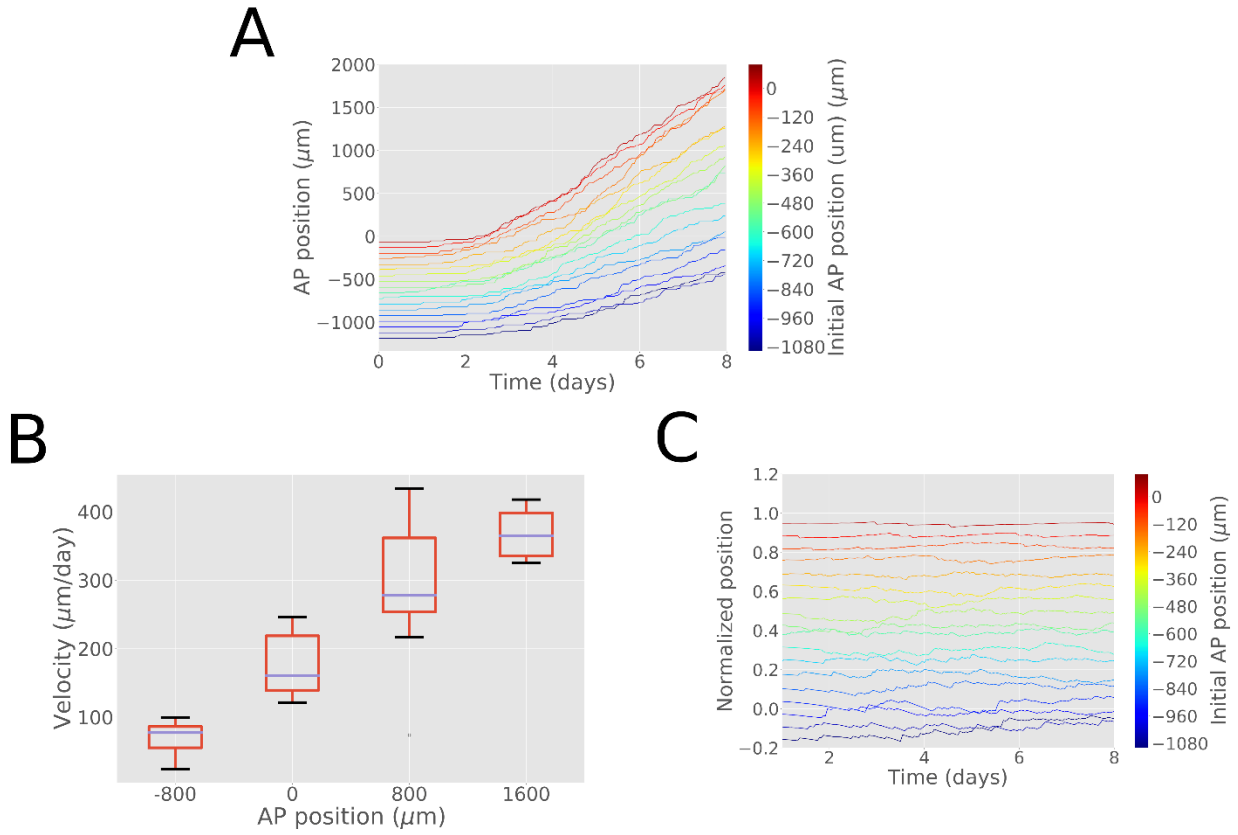

Figure 3. The model encompasses the cell pushing mechanism: the posterior a cell is, the faster it moves. A) Cells located close to the amputation plane end up at the posterior end of the regenerated modelled tissue. B) Clones velocity monotonically increases with AP coordinate. Box plot representation showing median of clone velocities binned every 800 μm **C) Scaling behavior: clone cells preserve their original spatial order.** Relative position of each clone to the highly proliferating tissue delimited by its outgrowth and the recruitment limit remains constant in time. The figure depicts 18 simulations.

S phase shortening is sufficient to explain the initial regenerative spinal cord outgrowth

Tail amputation in the axolotl triggers the shortening of both G1 and S phases, which leads to the acceleration of the cell cycle, and ultimately fast regenerative growth (Rodrigo Albors *et al.*, 2015). An important unknown is the relative contribution of each cell cycle phase to this outgrowth. We made use of our model to answer this question *in silico*. For this, we maintained the same parametrization recapitulating spinal cord outgrowth (Figure 2A and B) but modified the model such that recruited cells shorten S phase but not G1 phase (*i.e.*, leaving unaltered G1 phase) or *vice versa*. Interestingly, our results indicate that shortening of only S phase can explain the explosive spinal cord outgrowth observed *in vivo*, independently of G1 shortening, up to day 4 (Figure 4, green continuous line and red discontinuous line). In contrast, shortening of only G1 phase has a mild impact on the outgrowth, as it results in an outgrowth almost identical to the case in which neither G1 nor S phase were reduced (Figure 4, blue dotted line *versus* yellow line dot line). From day 4, though, shortening of only S phase cannot recapitulate the

observed outgrowth (Figure 4, green continuous line and red discontinues line) and indeed it is the shortening of both S and G1 phases what returns the same outgrowth than that observed *in vivo*. These modeling predictions are a consequence of the proximity of S phase to the next cell division (M phase), compared to G1 phase. To conclude, these results indicate that, up to day 4, shortening of S phase can explain the regenerative spinal cord outgrowth in the axolotl, while shortening of G1 is only evident to contribute to the regenerative growth from day 5.

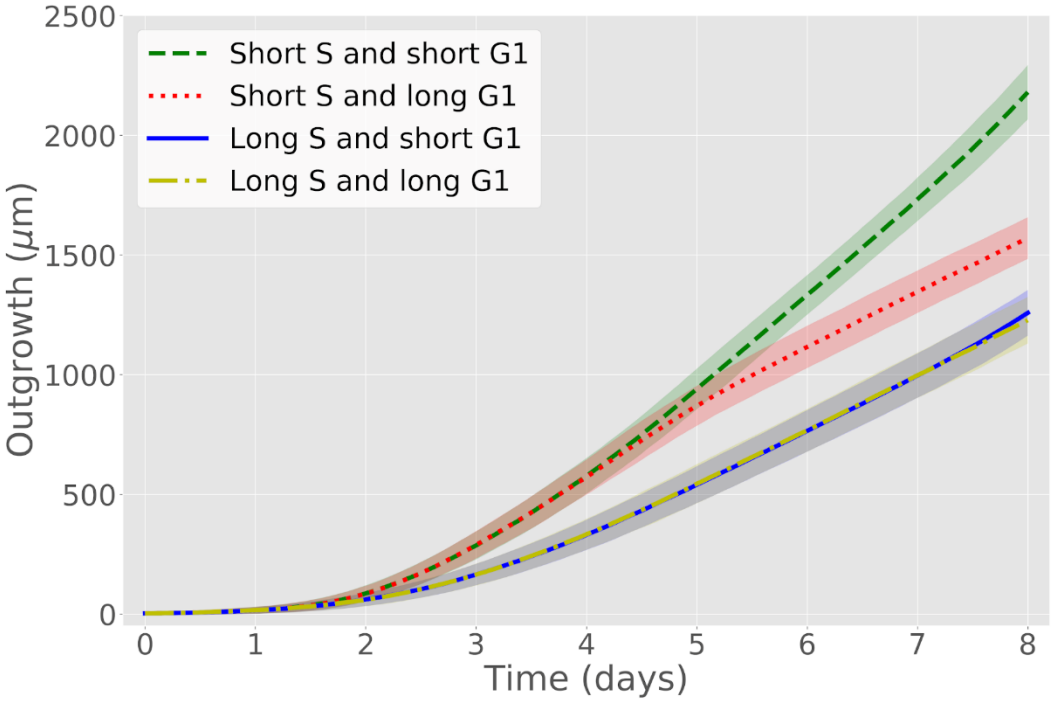

Figure 4. S phase shortening dominates cell cycle acceleration during axolotl spinal cord regeneration. Outgrowth kinetics predicted by the model assuming shortening of S and G1 phases (green), only shortening of S phase (red), only shortening of G1 phase (blue) and neither S nor G1 phases shortening (yellow). Means are represented as lines and each shaded area corresponds to one sigma out of 1,000 simulations.

Discussion

The tissue response to spinal cord injury differs greatly across vertebrates. In mammals, including humans, injuries to the spinal cord result in permanent tissue damage. In salamanders like the axolotl, the ependymal cell response is tightly orchestrated to faithfully rebuild the missing spinal cord (Joven & Simon, 2018; Tazaki, Tanaka & Fei, 2017). Following tail amputation, ependymal cells in the axolotl spinal cord switch from slow, neurogenic to faster, proliferative cell divisions (Rodrigo Albors *et al*., 2015). These faster cell cycles lead to the expansion of the ependymal/neural stem cell pool and drive an explosive regenerative growth. However, the mechanisms regulating cell cycle dynamics during spontaneous regeneration are not fully understood. Here, by using a modelling approach tightly linked to our previous experimental data, we find that the spatiotemporal pattern of cell proliferation during spinal cord regeneration in the axolotl is consistent with a signal that comes into play 24 hours post-amputation and recruits cells located within one millimeter anterior to the injury site. Moreover, we show that shortening of S phase is sufficient to explain the explosive growth observed during the first days of regeneration, but that both S and G1 shortening are necessary to explain/sustain the outgrowth during the expansion of the ependymal/neural stem cell pool (before the first new-born neurons are seen (Rodrigo Albors *et al*., 2015)).

Compared to the number of mathematical models designed to unveil pattern formation phenomena during development (Morelli *et al.*, 2012), modelling in regeneration is still in its infancy (Chara *et al*., 2014). An interesting example of modelling applied to regenerative processes was given by a system of deterministic ordinary differential equations that was superbly used to disentangle how secreted signaling factors could be used to control the output of multistage cell lineages in a self-renewing neural tissue, the mammalian olfactory epithelium (Lander *et al*., 2009). Another mathematical model based on ordinary differential equations was conceived to establish the causal relationship between the individually quantified cellular processes to unravel the stem cell dynamics in the developing spinal cord in chick and mouse (Kicheva *et al*., 2014). In a similar approach, we previously modelled the regenerating axolotl spinal cord by means of a system of deterministic ordinary differential equations describing the kinetics of the cycling and quiescent ependymal cell numbers which we mapped to a model of spinal cord outgrowth (Rost *et al*., 2016). This allowed us to conclude that while cell influx and cell cycle re-entry play a minor role, the acceleration of the cell cycle is the major driver of regenerative spinal cord outgrowth in axolotls (Rost *et al*., 2016). A more recent study based on ordinary and partial differential equations involving cell proliferation was used to predict the spinal cord growth of the knifefish (Ilieş, Sipahi & Zupanc, 2018).

In this follow-up study, we investigated the effect of the spatiotemporal distribution of cell proliferation during axolotl spinal cord regeneration. To do so, we developed a more general and yet accurate model introducing the spatial dimension relevant to the problem: the AP axis. To further build a more realistic model, we included non-deterministic attributes: a uniform distribution of the initial coordinates along the cell cycle and a normal distribution of the cell cycle length. In the model, a signal shortens the cell cycle of ependymal cells along the AP axis as a consequence of shortening their G1 and S phases, as we reported earlier (Rodrigo Albors *et al*., 2015). Regulation of G1 and S phases are a well-known mechanism controlling cell fate and cell output in a number of developmental contexts. In the brain, G1 lengthening results in longer cell cycles in neural progenitors undergoing neurogenesis (Lukaszewicz *et al.*, 2005; Calegari *et al*., 2005; Takahashi, Nowakowski & Caviness, 1995), while experimentally shortening of G1 in neural progenitors of the cerebral cortex results in more proliferative

269 divisions, increasing the progenitor pool and delaying neurogenesis (Salomoni & Calegari, 2010; Lange,
270 Huttner & Calegari, 2009; Pilaz *et al*., 2009; Calegari, F. & Huttner, 2003). Here, we have shown that the
271 shortening of G1 during spinal cord regeneration is necessary to sustain the expansion of the ependymal
272 cell pool. Together, these findings point to the regulation of G1 length as a key mechanism regulating the
273 output of neural stem/progenitor cell divisions in development and in regeneration. The length of S phase
274 is also regulated during development by modulating the number of DNA replication origins (Nordman &
275 Orr-Weaver, 2012). In mammals, shortening of S phase seems to play a role in the regulation of neuron
276 output: mouse neural progenitors committed to neurogenesis and neurogenic cortical progenitors in the
277 ferret undergo shorter S phase than their self-renewing/proliferative counterparts (Turrero García *et al*.,
278 2016; Arai *et al*., 2011). In regenerating ependymal cells of the axolotl, S phase shortens during the
279 expansion/outgrowth phase. Together, these findings suggest that the regulation of S phase controls cell
280 output in the context of development and regeneration but does not influence the mode of cell division.
281 In regenerating ependymal cells, it must be the combined shortening of S and G1 what leads to their initial
282 explosive (S shortening) expansion (G1 shortening) before resuming neurogenesis. In this line,
283 experimentally shortening G1 and S phases in cortical progenitors of the developing mouse brain delays
284 the onset of neurogenesis (Hasenpush-Theil *et al*., 2018). Our findings contribute to the evidences that
285 cell cycle regulation is a key mechanism controlling the amount and type of cells needed to generate and
286 regenerate a tissue.

287 Another prediction of our model is that a signal must spread about one millimeter from the injury
288 site to start recruiting ependymal cells 24 hours after amputation to explain the spatiotemporal pattern
289 of cell proliferation in the regenerating spinal cord. Since recruited cells share the same cell cycle length,
290 cell pushing causes homogeneous tissue expansion, which leads to scaling of their relative trajectories
291 (Averbukh *et al*., 2014). An important question now is whether the spatiotemporal distribution of this
292 potential signal agrees with the known signaling events operating during spinal cord regeneration.

293 A strong signal-recruiting candidate is the axolotl MARCKS-like protein (AxMLP), a secreted factor
294 involved in the proliferative response during axolotl appendage regeneration (Sugiura *et al*., 2016). AxMLP
295 is normally expressed in spinal cord cells but is upregulated following tail amputation, peaking 12 to 24 h
296 after amputation and returning to basal levels a day later (Sugiura *et al*., 2016). The time-course of AxMLP
297 expression thus fits within the timing prediction of our model and the secreted nature of AxMLP protein
298 could explain the long-range proliferative response in the regenerating spinal cord. In the future, a tighter
299 time-course characterization of AxMLP localization throughout axolotl spinal cord regeneration will help
300 putting our predictions to test.

301 Changes in the biophysical properties of the amputated tail could also trigger the orderly increase
302 in cell proliferation. In Xenopus tadpoles, tail amputation leads to the activation of the H+ V-ATPase which
303 is necessary and sufficient to promote tail regeneration (Adams *et al.*, 2007). In the axolotl, tail amputation
304 triggers changes in calcium, sodium, and membrane potential at the injury site (Ozkucur *et al*., 2010) while
305 spinal cord transection induces a rapid and dynamic change in the resting membrane potential which
306 drives a c-Fos dependent gene expression program promoting a pro-regenerative response (Sabin *et al*.,
307 2015). The proliferation-inducing signal could also be of mechanical nature (Chiou & Collins, 2018). In this
308 direction, it is interesting that spinal cord transection in the zebrafish induces an immediate alteration in
309 the mechanical properties in the lesion site, which gradually returns to normal (Schlüßler *et al*., 2018).
310 Our predictions of the temporal and spatial distribution that such proliferation-inducing signal could have
311 will guide efforts to narrow down the mechanisms responsible for successful spinal cord regeneration.

Taken together, our study provides a finer mechanistic understanding of the cell cycle kinetics that drive spinal cord regeneration in axolotl and paves the way to search for the signal or signals that launch the successful ependymal cell response to spinal cord injury.

316 **4. Computational methods**

317 **Model of developing and regenerating axolotl spinal cord**

318 We modeled the spinal cord as a densely-packed row of ependymal cells. Since all the cells are assumed
319 identical rigid spheres, the model effectively involves only one spatial dimension: the anterior-posterior
320 (AP) axis of the spinal cord. We assumed that each cell proliferates with a certain random cell cycle length
321 T_C. The cell cycle length T_C is assumed normally distributed (T_C = N (μ_{TC}, σ_{TC})). In the initial condition, each
322 cell is in a random coordinate χ (t = 0) = χ_0 along its particular cell cycle, where χ_0 is assumed uniformly
323 distributed between zero and its corresponding T_C. As time goes by, each cell moves its cell coordinate χ
324 (t) deterministically until it reaches its corresponding T_C value. At this precise moment, the cell divides and
325 one daughter inherits its mother's AP coordinate while the other is intercalated between the first
326 daughter and the posterior neighboring cell. This last feature of the model is the implementation of what
327 we earlier defined as "cell pushing mechanism" (Rost *et al*., 2016). This model predicts that after a time
328 of approximately one cell cycle length, mitotic events will occur along the AP axis, contributing to the
329 growth of the spinal cord during development (Figure 1A).

330 To study the evolution of the tissue under a regenerative setup, we focused on the tissue response
331 to an amputation modeled by simply removing the most posterior N_r cells. We modeled the regenerative
332 response in the remaining N_0 cells by assuming that amputation triggers the release of a signal, which
333 spreads over the AP axis a distance of λ μm anterior to the amputation plane and, after a time τ, recruits
334 the ependymal cells within the λ μm zone, inducing a change in their proliferation program. Because
335 regenerative ependymal cells go through shorter G1 and S phases of the cell cycle than non-regenerative
336 ependymal cells (Rodrigo Albors *et al*., 2015), we assumed that the released signal instructs regenerating
337 ependymal cells precisely to reduce G1 and S phases, effectively shortening their cell cycle.

338 We notated the AP position of the most anterior cell recruited by the signal as $\xi(t)$, the recruitment
339 limit, such that $\xi(t = \tau) = \lambda$. Note that before $t = \tau$ there is not recruitment limit since all ependymal cells
340 within the AP axis proliferate with the same T_C. Hence, for $t = \tau$, all the cells anterior to the cell located at
341 $\xi(t)$ are not recruited and continue cycling slowly during the simulations (Figure 1-figure supplement 1B).
342 In contrast, at the same time, cells posterior to $\xi(t)$, and thus located within λ μm anterior to the
343 amputation plane, are instantaneously recruited. This means that the cell cycle coordinates of these cells
344 undergo a coordinate transformation, modifying their cycling according to the cell cycle phase in which
345 they are in: if the cell cycle coordinate at $t = \tau$ belongs to G2 or M, the cell will continue cycling as before
346 (Figure 1-figure supplement 1B). If the cell cycle coordinate belongs to G1, we considered the following
347 mechanism (Figure 1-figure supplement 1B): If the recruited cell has a cell cycle coordinate which is lower
348 than certain critical coordinate $G1_{cr}$ when $t = \tau$, its cell cycle coordinate will be equal to $G1_{cr}$ in the next
349 simulation step. If the cell cycle coordinate of the recruited cell is higher than $G1_{cr}$ when $t = \tau$, it will
350 continue cycling as before. This mechanism induces a partial synchronization of cells transiting through
351 G1. (Figure 1C and Figure 1-figure supplement 1B). Finally, if the cell cycle coordinate belongs to S when t
352 $= \tau$, we assumed a proportional mapping mechanism: the new cell cycle coordinate of this cell will be
353 proportionally mapped to the corresponding coordinate of a shortened S phase in the next simulation
354 step (Figure 1C and Figure 1-figure supplement 1B).

355 Finally, daughter cells of recruited cells maintain shortened G1 and S phases as their mothers and
356 consequently have shorter cell cycle lengths (Figure 1C).

357

358 **Model parametrization**

359 The model parameters are summarized in Table 1. Briefly, the ependymal cell length along the AP axis and
360 the distributions of cell phases durations and cell lengths were fixed from our previous publication
361 (Rodrigo Albors *et al.*, 2015). The only free model parameters are the remaining anterior cells after
362 amputation N_0, the length λ along the AP axis of the putative signal and τ, the time between amputation
363 and cell recruitment.

364

365 **Fitting procedure of the experimental switchpoint with the theoretical recruitment limit $\xi(t)$**

366 The experimentally obtained switchpoint of the regenerating axolotl spinal cord (extracted from Rost *et*
367 *al.*, 2016) was fitted with the model-predicted recruitment limit $\xi(t)$. Free model parameters N_0, λ and τ
368 were estimated by sweeping N_0 from 100 to 300 (with a sampling of 5) and λ from 500 to 1,500 (with a
369 sampling of 50) and τ from 0 to 192 (with sampling of 6). For each combination of parameters, we
370 performed 1,000 replicated simulations from 1,000 random seeds. Best fitting result was estimated by
371 minimization of the residual sum of squares between the means of the experimental switchpoint and the
372 simulated recruitment limit $\xi(t)$. Implementation of the recruitment limit $\xi(t)$ and its fitting to the
373 experimental switchpoint are available in 'main/Simulating_recruitment_limit.ipynb' and
374 'main/Fitting_recruitment_limit.ipynb', respectively, in Cura Costa *et al.*, 2020a.

375

376 **Clones trajectories**

377 We calculated the clone trajectories following the positions of each clone in random simulations. When a
378 cell divided, we kept the mean position of the clone cells as the clone position. In Figure 3A, a total of 18
379 tracks are shown, the first trajectory starts at 0 (the amputation plane) and the last at -1100 µm (with a
380 sampling of 50 µm, approximately). Calculations of clone trajectories are available in the
381 'figures/Fig_3A.ipynb' in Cura Costa *et al.*, 2020a.

382

383 **Clones velocities**

384 To estimate the mean velocity of clones at different spatial positions in this model, the space along the
385 AP axis was subdivided into 800 µm bins. For each clone trajectory, the positions were grouped according
386 to these bins. Groups containing less than two measurements were excluded. The average clone velocity
387 for each group was estimated with linear regression. Then, the mean and standard deviation of the
388 velocity of all the clones in a bin was calculated. Calculations of clone velocities are available in the
389 'figures/Fig_3B.ipynb' in Cura Costa *et al.*, 2020.

390

391

392

Coordinate system

In all our simulations, the time starts with the event of amputation. Space corresponds to the anterior-posterior (AP) axis, where 0 represents the amputation plane and positive (negative) values are posterior (anterior) locations.

Model implementation and computational tools

The models were implemented in Python 3.0. Simulations and data analysis were performed using Numpy (Oliphant, 2006) and Pandas (McKinney, 2010) while data visualization was executed with Matplotlib (Hunter, 2007).

Supplementary notebooks

Jupyter Notebook (http://jupyter.org/) containing the source code for all computations performed and referred to as Cura Costa *et al.*, 2020a in this study can be found at https://doi.org/10.5281/zenodo.3647640.

Acknowledgements

We thank Fabian Rost for critical comments on the manuscript. We also thank the members of the Chara lab for interesting discussions.

Funding

This work was funded by Consejo Nacional de Investigaciones Científicas y Técnicas (CONICET) of Argentina and by the grants from Agencia Nacional de Promoción Científica y Tecnológica (ANPCyT), PICT-2014-3469 and PICT-2017-2307 to O.C. E.C.C. was supported by a doctoral scholarship program from CONICET. O.C. is a career researcher from CONICET. A.R.A. was supported by the European Union's Horizon 2020 research and innovation programme under the Marie Skłodowska-Curie grant agreement No 753812.

420 **References**

421 Adams DS, Masi A & Levin M. 2007. H+ Pump-dependent changes in membrane voltage are an early
422 mechanism necessary and sufficient to induce Xenopus tail regeneration. Development. 34(7): 1323-35.

423 Arai Y, Pulvers JN, Haffner C, Schilling B, Nüsslein I, Calegari F, Huttner WB. 2011. Neural stem and
424 progenitor cells shorten S-phase on commitment to neuron production. Nat Commun. 2:154.

425 Averbukh I, Ben-Zvi D, Mishra S & Barkai N. 2014. Scaling morphogen gradients during tissue growth by
426 a cell division rule. Development. 141(10): 2150-6.

427 Becker CG, Becker T, Hugnot JP. 2018. The spinal ependymal zone as a source of endogenous repair cells
428 across vertebrates. Prog Neurobiol. 170: 67-80.

429 Calegari F & Huttner WB. 2003. An inhibition of cyclin-dependent kinases that lengthens, but does not
430 arrest, neuroepithelial cell cycle induces premature neurogenesis. J Cell Sci. 116: 4947–4955.

431 Calegari F, Haubensak W, Haffner C, Huttner WB. 2005. Selective lengthening of the cell cycle in the
432 neurogenic subpopulation of neural progenitor cells during mouse brain development. J Neurosci.
433 25(28): 6533-8.

434 Chara O, Tanaka EM & Brusch L. 2014. Mathematical modeling of regenerative processes. Curr Top Dev
435 Biol. 108: 283-317.

436 Chernoff EA, Stocum DL, Nye HL, Cameron JA. 2003. Urodele spinal cord regeneration and related
437 processes. Dev Dyn. 226(2): 295-307.

438 Chiou K & Collins ES. 2018. Why we need mechanics to understand animal regeneration. Dev Biol.
439 433(2): 155-165.

440 Fei JF, Schuez M, Tazaki A, Taniguchi Y, Roensch K & Tanaka EM. 2014. CRISPR-mediated genomic
441 deletion of Sox2 in the axolotl shows a requirement in spinal cord neural stem cell amplification during
442 tail regeneration. Stem Cell Reports. 3(3): 444-59.

443 Freitas PD, Yandulskaya AS & Monaghan JR. 2019. Spinal Cord Regeneration in Amphibians: A Historical
444 Perspective. Dev Neurobiol. 79(5): 437-452.

445 Hasenpusch-Theil K, West S, Kelman A, Kozic Z, Horrocks S, McMahon AP, Price DJ, Mason JO, Theil T.
446 2018. Gli3 controls the onset of cortical neurogenesis by regulating the radial glial cell cycle through
447 Cdk6 expression. Development. 145(17).

448 Hunter JD. 2007. Matplotlib: A 2D graphics environment. Computing in Science & Engineering. 9:90–95.

449 Ilieş I, Sipahi R & Zupanc GKH. 2018. Growth of adult spinal cord in knifefish: development and
450 parametrization of a distributed model. Journal of Theoretical Biology. 437: 101–114.

451 Joven A & Simon A. 2018. Homeostatic and regenerative neurogenesis in salamanders. Prog Neurobiol.
452 170: 81-98.

453 Kicheva A, Bollenbach T, Ribeiro A, Valle HP, Lovell-Badge R, Episkopou V & Briscoe J. 2014. Coordination
454 of progenitor specification and growth in mouse and chick spinal cord. Science 345: 1254927.

455 Lander AD, Gokoffski KK, Wan FY, Nie Q & Calof AL. 2009. Cell lineages and the logic of proliferative
456 control. PLoS Biol. 7(1): e15.

457 Lange C, Huttner WB & Calegari F. 2009. Cdk4/cyclinD1 overexpression in neural stem cells shortens G1,
458 delays neurogenesis, and promotes the generation and expansion of basal progenitors. Cell Stem Cell.
459 5(3): 320-31.

460 Lukaszewicz A, Savatier P, Cortay V, Giroud P, Huissoud C, Berland M, Kennedy H & Dehay C. 2005. G1
461 phase regulation, area-specific cell cycle control, and cytoarchitectonics in the primate cortex. Neuron
462 47: 353–364.

463 McKinney W. 2010. Data structures for statistical computing in Python. Proceedings of the 9th Python in
464 Science Conference: 51-56.

465 Morelli LG, Uriu K, Ares S & Oates AC. 2012. Computational approaches to developmental patterning.
466 Science. 336(6078): 187-91.

467 Nordman J & Orr-Weaver TL. 2012. Regulation of DNA replication during development. Development
468 139: 455-464.

469 Oliphant TE. 2006. A guide to NumPy, USA: Trelgol Publishing.

470 Ozkucur N, Epperlein HH & Funk RH. 2010. Ion imaging during axolotl tail regeneration in vivo. Dev Dyn.
471 239(7): 2048-57.

472 Pilaz LJ, Patti D, Marcy G, Ollier E, Pfister S, Douglas RJ, Betizeau M, Gautier E, Cortay V, Doerflinger N,
473 Kennedy H & Dehay C. 2009. Forced G1-phase reduction alters mode of division, neuron number, and
474 laminar phenotype in the cerebral cortex. Proc Natl Acad Sci U S A. 106(51): 21924-9.

475 Rodrigo Albors A, Tazaki A, Rost F, Nowoshilow S, Chara O & Tanaka EM. 2015. Planar cell polarity-
476 mediated induction of neural stem cell expansion during axolotl spinal cord regeneration. eLife. 4:
477 e10230.

478 Rost F, Rodrigo Albors A, Mazurov V, Brusch L, Deutsch A, Tanaka EM & Chara O. 2016. Accelerated cell
479 divisions drive the outgrowth of the regenerating spinal cord in axolotls. eLife. 5. pii: e20357.

480 Sabin K, Santos-Ferreira T, Essig J, Rudasill S & Echeverri K. 2015. Dynamic membrane depolarization is
481 an early regulator of ependymoglial cell response to spinal cord injury in axolotl. Dev Biol. 408(1): 14-25.

482 Salomoni P & Calegari F. 2010. Cell cycle control of mammalian neural stem cells: putting a speed limit
483 on G1. Trends Cell Biol. 20: 233–243.

484 Schlüßler R, Möllmert S, Abuhattum S, Cojoc G, Müller P, Kim K, Möckel C, Zimmermann C, Czarske J &
485 Guck J. 2018. Mechanical Mapping of Spinal Cord Growth and Repair in Living Zebrafish Larvae by
486 Brillouin Imaging. Biophys J. 115(5): 911-923.

487 Sugiura T, Wang H, Barsacchi R, Simon A & Tanaka EM. 2016. MARCKS-like protein is an initiating
488 molecule in axolotl appendage regeneration. Nature. 531(7593): 237-40.

489 Takahashi T, Nowakowski RS & Caviness VS Jr. 1995. The cell cycle of the pseudostratified ventricular
490 epithelium of the embryonic murine cerebral wall. J Neurosci. 15(9): 6046-57.

491 Tazaki A, Tanaka EM & Fei JF. 2017. Salamander spinal cord regeneration: The ultimate positive control
492 in vertebrate spinal cord regeneration. Dev Biol. 432(1): 63-71.

493 Turrero García M, Chang Y, Arai Y & Huttner WB. 2016. S-phase duration is the main target of cell cycle
494 regulation in neural progenitors of developing ferret neocortex. J Comp Neurol. 524(3): 456-70.

Supplementary Figures

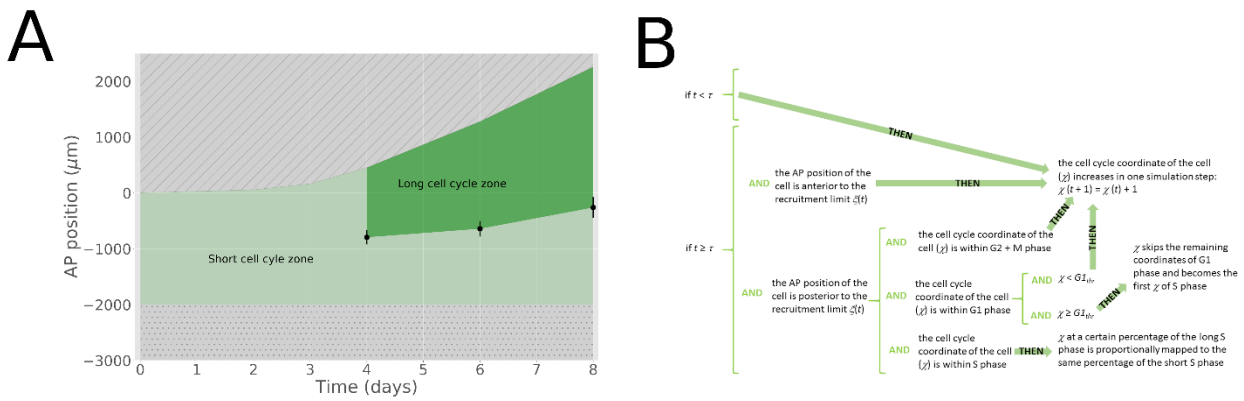

Figure 1-figure supplement 1. A) Space-time distribution of cell proliferation during axolotl spinal cord regeneration. Experimental switchpoint (black dots) separating areas of low (light-green) from high (dark-green) cell proliferation along the anterior-posterior (AP) axis of the axolotl spinal cord. The dashed region marks the space outside of the embryo while the dotted region marks the unaffected part of the embryo (adapted from Fig.2 F'' of Rost *et al*., 2016). **B) Schematic of the model of cell recruitment by shortening G1 and S phase.** The cartoon shows how cell cycle coordinates of ependymal cells undergo a coordinate transformation, modifying their cycling according to the cell cycle phase in which they are in.

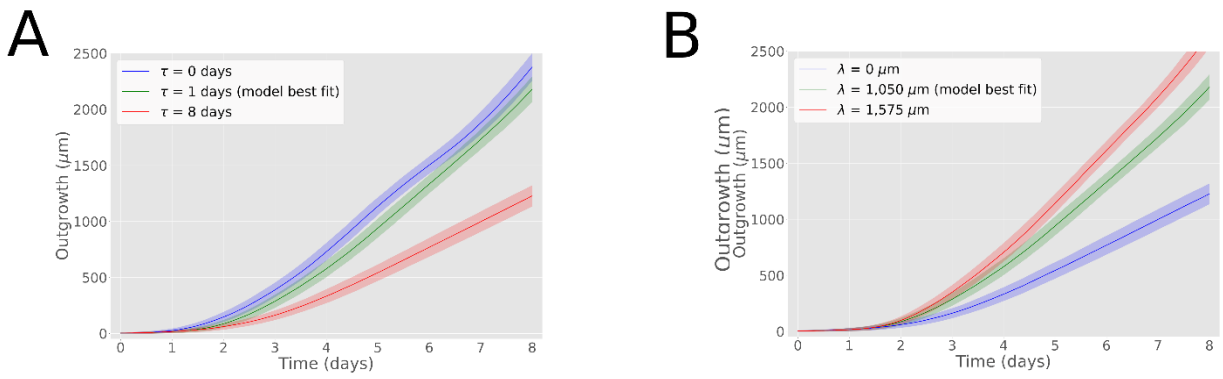

Figure 2-figure supplement 2. The delay between amputation and cell recruitment (τ) and the initial recruitment length (λ) determine the outgrowth of the axolotl spinal cord. A) Increase of τ reduces the model-predicted spinal cord outgrowth. Time course of spinal cord outgrowth predicted by the model when varying τ from zero (blue) to 8 days (red). In green, the prediction of the model assuming τ = 1 day. N_0 = 200 cells and λ = 1,050 μm. **B) Increase of λ increases the model-predicted spinal cord outgrowth.** Time course of spinal cord outgrowth predicted by the model when varying λ from zero (blue) to 1,575 μm (red). In green, the prediction of the model assuming λ = 1,050 day. N_0 = 200 cells and τ = 1 day. Simulations depicted in the green curves in A and B are the same simulations shown in Fig. 2 B. In A and B, the means are depicted as lines while dark and light shaded areas correspond to 95 and 99.7 % confidence intervals, respectively, calculated from 1000 simulations.

Movies

Movie M1. 1D Model simulations of spinal cord regeneration. **Top panel)** 20 model simulations from 20 different random seeds. The color code corresponds to the generation of each cell (orange, light green, medium green, dark green, and black correspond to the first, second, third, four and fifth generation, respectively). Vertical interrupted black line denotes the amputation plane (AP coordinate of 0). At 24 hpa the region of -1,050 μm from the amputation plane is highlighted in red indicating the λ μm delimited by the recruitment limit ξ(t), which moves posteriorly thereafter as a dashed and dotted red line. **Bottom left panel)** Predicted recruitment limit ξ(t) as a function of time from the simulations showed in A). Mean value is depicted in the red line while the red shaded areas corresponds to 95 and 99.7 % confidence intervals **Bottom right panel)** Predicted spinal cord outgrowth predicted by the model from the simulations showed in A). The line represents to the mean and the green shaded areas, from darker to lighter, correspond to the 68, 95 and 99.7 % confidence intervals. The 20 simulations have the same parametrization than the 1,000 simulations showed in Fig. 2 A and Fig. 2 B.

533 **Tables**

534

535 **Table 1.** Model parameters.

Model parameter	Value / explanation	Fixed/Free
G1 phase non-regenerating mean	152 hours	Fixed parameters, extracted from Rodrigo Albors *et al.*, 2015.
G1 phase non-regenerating sigma	54 hours	
S phase non-regenerating mean	179 hours	
S phase non-regenerating sigma	21 hours	
G2 + M phases non-regenerating mean	9 hours	
G2 + M phases non-regenerating sigma	6 hours	
G1 phase regenerating mean	22 hours	
G1 phase regenerating sigma	19 hours	
$G1_{cr}$	130 hours	
S phase regenerating mean	88 hours	
S phase regenerating sigma	9 hours	
G2 + M phases regenerating mean	9 hours	
G2 + M phases regenerating sigma	2 hours	
Cell length along the AP axis	13.2 μm	
N_0	Initial number of cells along the AP axis, anterior to the amputation plane.	Free parameters (determined in this study).
λ	Length from the amputation plane recruited by the signal (μm).	
τ	Delay between the moment of amputation and cell recruitment (days after amputation or hours after amputation).	

536